AIAA AVIATION Forum
June 15-19, 2020, VIRTUAL EVENT
AIAA AVIATION 2020 FORUM

10.2514/6.2020-3013

Improved Delayed Detached Eddy Simulation of Separated Flow

Purvic Patel* and Gecheng Zha†
Dept. of Mechanical and Aerospace Engineering
University of Miami, Coral Gables, Florida 33124
E-mail: gzha@miami.edu

The SST based Improved Delayed Detached Eddy Simulation (IDDES) is implemented and utilized with a 3D compressible Navier-Stokes solver to investigate the physics of flow separation. The implementation is first validated with the standard zero pressure gradient subsonic flat plate case and the results agree well with the SST model prediction. After the validation, the wall-mounted NASA hump and NACA 0012 airfoil post-stall flow cases are simulated with the SST and SST-IDDES. The high-fidelity IDDES predicts the separation size as well as the aerodynamic performance in close agreement with the experiment. Apart from the quantitative results, its efficacy is also observed in more realistic 3-D turbulent flow structures.

I. Nomenclature

L_∞	=	Reference length
ρ_∞	=	Freestream density
U_∞	=	Freestream velocity
μ_∞	=	Freestream dynamics viscosity
c_∞	=	Freestream speed of sound
d	=	Distance from the nearest wall
$\mathbf{l}, \mathbf{m}, \mathbf{n}$	=	Surface area vector in ξ, η and ζ direction respectively
$\mathbf{\Omega}$	=	Vorticity
Re	=	Reynolds number
$i,\ j,\ k$	=	Dummy indices for Indicial / Einstein summation notation
κ	=	von Karmann constant
δ_{ij}	=	Kronecker delta
Δt	=	Physical time step
$U,\ V,\ W$	=	Contravariant velocities in ξ, η and ζ directions
k	=	Turbulence kinetic energy (k)
ϵ	=	Turbulence dissipation rate (ϵ)
ω	=	Turbulence specific dissipation rate (ω)
RANS	=	Reynolds Averaged Navier Stokes
SA	=	Spalart-Allmaras
SST	=	Shear Stress Transport
DES	=	Detached Eddy Simulation
DDES	=	Delayed Detached Eddy Simulation
IDDES	=	Improved Delayed Detached Eddy Simulation

II. Introduction

A flow separation for high Reynolds number turbulent flow poses a challenge to Favre/Reynolds Averaged Navier Stokes (FANS/RANS) equations with a turbulence model. The reason is that a RANS model intends to model the entire turbulent spectrum using the statistical time-averaged flow description. The RANS approach is widely used for the attached flow due to its superiority in terms of speed and computational resources over Direct Numerical Simulation

*Ph.D. Candidate
†Professor, ASME Fellow, AIAA associate Fellow.

(DNS) and Large Eddy Simulation (LES). An unsteady RANS (URANS) with an additional unsteady term performs better than steady RANS for the cases with long-term periodical oscillations. However, it still fails to predict the separation accurately in many cases as it does not account for the energy associated with the different turbulent length scales.

In Large Eddy Simulation (LES), time-dependent compressible Navier-Stokes equations are Favre filtered. The large scale eddies containing most of the turbulent energy are resolved, whereas small scale isotropic eddies are modeled. This approach makes LES prediction more general in comparison to URANS models and reveals more flow physics. To resolve the boundary layer, LES requires very fine mesh near the wall and smaller time-step. This makes LES too expensive for high Reynolds number industrial problems even with the current advances in computational resources.

A hybrid turbulence model is a stride in the direction of bridging two streams, namely RANS and LES, in a single model to simulate turbulent flow by taking advantage of both approaches. Near the wall, the boundary layer is modeled with its RANS mode and therefore, it circumvents high mesh resolution requirement of the LES model there. Outside the boundary layer or away from the wall, it performs in the LES mode and resolves large-energy containing eddies. This unique capability allows it to perform better than the URANS under mild or massive flow separation.

Several hybrid turbulence models have been proposed within the last two decades and the Detached Eddy Simulation (DES) based models have widely gained the attention of researchers for the separated flow. The history of the DES-based model goes back to the DES97 proposed by Spalart et al. [1] in 1997. This hybrid model is developed based on the Spalart-Allmaras (SA) one-equation model, where the switch from RANS to LES explicitly depends on the local grid size. Strelets [2] proposed the DES formulation based on the SST model by redefining the length scale of the model and describing the destruction term of turbulence kinetic energy in terms of this modified length scale. The explicit switch necessitates following the rigorous mesh refinement guidelines to avoid the Grid Induced Separation (GIS) [3, 4]. Menter et al. [5] proposed a zonal SST-DES model by shielding the boundary layer from the DES limiter. This model circumvents the GIS problem; however, the wall parallel spacing should not fall below $0.1\delta_{||}$. Spalart et al. [4] later proposed non-zonal Delayed Detached Eddy Simulation (DDES) deriving an idea of shielding the boundary layer from Menter et al. [5]. His formulation can be used with any model involving eddy viscosity and a shielding function depends on the eddy viscosity and the nearest wall distance. Later Shur et al. [6] proposed Improved Delayed Detached Eddy Simulation (IDDES) to address the Logarithmic Layer Mismatch (LLM) problem between the inner RANS and the outer LES due to the use of original DES as a WMLES formulation. Although the shielding functions proposed for DDES and IDDES by Spalart et al. [4] and Shur et al. [6] respectively are generic, they are calibrated based on the one-equation SA turbulence model. Gritskevich et al. [7] revisited and recalibrated these functions in combination with the SST turbulence model.

In this paper, the IDDES based on the SST turbulence model is utilized with a high-order numerical scheme to simulate some flow separation problems. The implementation of SST-IDDES is first validated with the standard zero-gradient subsonic flat plate case. After that, two cases are examined, namely 2-D NASA hump and post-stall flow of NACA0012 airfoil. In these cases, a RANS model over-predicts either the separation size or the aerodynamic performance. The predicted results with the SST-IDDES approach agrees well with the experiment as compared to the SST model.

III. Turbulence Modeling

The Favre-filtered Navier-Stokes equation along with the Improved Delayed Detached Eddy Simulation (IDDES) based on the SST-2003 turbulence model are solved in a fully coupled manner using an implicit unfactored Gauss-Seidel line iteration [8]. The Favre-filtered equations are nondimensionalized using L_∞, ρ_∞, U_∞ and μ_∞ and their differential form in generalized coordinates is given by:

$$\frac{\partial \mathbf{Q}}{\partial t} + \frac{\partial \mathbf{E}}{\partial \xi} + \frac{\partial \mathbf{F}}{\partial \eta} + \frac{\partial \mathbf{G}}{\partial \zeta} = \frac{1}{Re}\left[\frac{\partial \mathbf{R}}{\partial \xi} + \frac{\partial \mathbf{S}}{\partial \eta} + \frac{\partial \mathbf{T}}{\partial \zeta}\right] + \mathbf{D} \tag{1}$$

where,

$$
\begin{aligned}
\mathbf{Q} &= \frac{1}{J}\mathbf{Q}' \\
\mathbf{E} &= \frac{1}{J}\left(\mathbf{Q}'\xi_t + \mathbf{E}'\xi_x + \mathbf{F}'\xi_y + \mathbf{G}'\xi_z\right) = \frac{1}{J}\left(\mathbf{Q}'\xi_t + \mathbf{E}''\right) \\
\mathbf{F} &= \frac{1}{J}\left(\mathbf{Q}'\eta_t + \mathbf{E}'\eta_x + \mathbf{F}'\eta_y + \mathbf{G}'\eta_z\right) = \frac{1}{J}\left(\mathbf{Q}'\eta_t + \mathbf{F}''\right) \\
\mathbf{G} &= \frac{1}{J}\left(\mathbf{Q}'\zeta_t + \mathbf{E}'\zeta_x + \mathbf{F}'\zeta_y + \mathbf{G}'\zeta_z\right) = \frac{1}{J}\left(\mathbf{Q}'\zeta_t + \mathbf{G}''\right) \\
\mathbf{R} &= \frac{1}{J}\left(\mathbf{R}'\xi_x + \mathbf{S}'\xi_y + \mathbf{T}'\xi_z\right) \\
\mathbf{S} &= \frac{1}{J}\left(\mathbf{R}'\eta_x + \mathbf{S}'\eta_y + \mathbf{T}'\eta_z\right) \\
\mathbf{T} &= \frac{1}{J}\left(\mathbf{R}'\zeta_x + \mathbf{S}'\zeta_y + \mathbf{T}'\zeta_z\right) \\
\mathbf{D} &= \frac{1}{J}\mathbf{D}'
\end{aligned}
\tag{2}
$$

Here, J is the transformation jacobian. The conservative variable vector $\mathbf{Q}'$ is expressed as:

$$
\mathbf{Q}' = \begin{pmatrix} \rho \\ \rho u \\ \rho v \\ \rho w \\ \rho e \\ \rho k \\ \rho \omega \end{pmatrix} \tag{3}
$$

The inviscid flux vectors, i.e., $\mathbf{E}$, $\mathbf{F}$, and $\mathbf{G}$, represent the inviscid flux through the cell interface with normals in the positive ξ, η, and ζ directions, respectively. They are written as:

$$
\mathbf{E} = \begin{pmatrix} \rho U \\ \rho u U + l_x p \\ \rho v U + l_y p \\ \rho w U + l_z p \\ (\rho e + p)U - l_t p \\ \rho k U \\ \rho \omega U \end{pmatrix}, \ \mathbf{F} = \begin{pmatrix} \rho V \\ \rho u V + m_x p \\ \rho v V + m_y p \\ \rho w V + m_z p \\ (\rho e + p)V - m_t p \\ \rho k V \\ \rho \omega V \end{pmatrix}, \ \mathbf{G} = \begin{pmatrix} \rho W \\ \rho u W + n_x p \\ \rho v W + n_y p \\ \rho w W + n_z p \\ (\rho e + p)W - n_t p \\ \rho k W \\ \rho \omega W \end{pmatrix} \tag{4}
$$

Here, $\mathbf{l}$, $\mathbf{m}$, $\mathbf{n}$ represent the normal vectors with their magnitudes equal to the elemental surface areas and pointing in the positive ξ, η, ζ directions respectively. The contravariant velocities (Eq. (5)) through each cell interface are defined as:

$$
\begin{aligned}
U &= l_t + \mathbf{l} \bullet \mathbf{V} = l_t + l_x u + l_y v + l_z w \\
V &= m_t + \mathbf{m} \bullet \mathbf{V} = m_t + m_x u + m_y v + m_z w \\
W &= n_t + \mathbf{n} \bullet \mathbf{V} = n_t + n_x u + n_y v + n_z w
\end{aligned}
\tag{5}
$$

where,

$$
\mathbf{l} = \frac{\nabla \xi}{J}, \ \mathbf{m} = \frac{\nabla \eta}{J}, \ \mathbf{n} = \frac{\nabla \zeta}{J} \tag{6}
$$

and the grid moving velocities are defined as,

$$
l_t = \frac{\xi_t}{J}, \ m_t = \frac{\eta_t}{J}, \ n_t = \frac{\zeta_t}{J} \tag{7}
$$

The dimensionless pressure p is related with the dimensionless density ρ, total energy e, velocity components u, v, w and turbulence kinetic energy k as,

$$p = (\gamma - 1)\left[\rho e - \frac{1}{2}\rho\left(u^2 + v^2 + w^2\right) - \rho k\right] \tag{8}$$

The perfect gas equation of state and speed of sound (c) is written in the dimensionless form as,

$$\begin{aligned} T &= \frac{\gamma M_\infty^2 p}{\rho} \\ c^2 &= \frac{\gamma p}{\rho} \end{aligned} \tag{9}$$

Similarly to the inviscid flux vectors, **R**, **S**, and **T** are the viscous flux vectors in the respective direction and they are written as:

$$\mathbf{R} = \begin{pmatrix} 0 \\ l_k\tau_{xk} \\ l_k\tau_{yk} \\ l_k\tau_{zk} \\ l_kQ_k \\ (\mu + \sigma_k\mu_t)(\mathbf{l} \bullet \nabla k) \\ (\mu + \sigma_\omega\mu_t)(\mathbf{l} \bullet \nabla \omega) \end{pmatrix}, \ \mathbf{S} = \begin{pmatrix} 0 \\ m_k\tau_{xk} \\ m_k\tau_{yk} \\ m_k\tau_{zk} \\ m_kQ_k \\ (\mu + \sigma_k\mu_t)(\mathbf{m} \bullet \nabla k) \\ (\mu + \sigma_\omega\mu_t)(\mathbf{m} \bullet \nabla \omega) \end{pmatrix}, \ \mathbf{T} = \begin{pmatrix} 0 \\ n_k\tau_{xk} \\ n_k\tau_{yk} \\ n_k\tau_{zk} \\ n_kQ_k \\ (\mu + \sigma_k\mu_t)(\mathbf{n} \bullet \nabla k) \\ (\mu + \sigma_\omega\mu_t)(\mathbf{n} \bullet \nabla \omega) \end{pmatrix} \tag{10}$$

The total shear stress (τ_{ik}) and the total heat flux (q_j) for turbulent flow are given by:

$$\begin{aligned} \tau_{ik} &= (\mu + \mu_t)\left[\left(\frac{\partial u_i}{\partial x_k} + \frac{\partial u_k}{\partial x_i}\right) - \frac{2}{3}\delta_{ik}\frac{\partial u_j}{\partial x_j}\right] - \frac{2}{3}\delta_{ik}\rho k Re \\ q_j &= -\frac{1}{(\gamma - 1)\, M_\infty^2}\left(\frac{\mu}{\mathrm{Pr}} + \frac{\mu_t}{\mathrm{Pr}_t}\right)\frac{\partial T}{\partial x_j} \end{aligned} \tag{11}$$

where, μ is the molecular viscosity and it is calculated using the Sutherlands law. The turbulent viscosity μ_t is computed based on the SST-IDDES turbulence model.

The source term vector, $\mathbf{D}'$, includes the SST-IDDES model source terms here. In the case of turbomachinery, this vector may carry extra terms for momentum equations depending on the frame of reference.

$$\mathbf{D}' = \begin{pmatrix} 0 \\ 0 \\ 0 \\ 0 \\ 0 \\ \tilde{P_k} - D_k \\ P_\omega - D_\omega + CD_\omega \end{pmatrix} \tag{12}$$

The production limiter is used to avoid the turbulence built-up in the stagnation regions. For the IDDES capability, the destruction term (D_k) of the SST-2003 is modified based on Gritskevich et al. [7]. The production ($\tilde{P_k}$) and destruction (D_k) term of the turbulent kinetic energy (k) are given by:

$$\begin{aligned} P_k &= \frac{1}{Re}\left[\mu_t\left(\frac{\partial u_i}{\partial x_j} + \frac{\partial u_j}{\partial x_i} - \frac{2}{3}\delta_{ij}\frac{\partial u_k}{\partial x_k}\right) - \frac{2}{3}\rho k\delta_{ij}Re\right]\frac{\partial u_i}{\partial x_j} \\ \tilde{P_k} &= \min(P_k, 10\beta^*\rho\omega k) \\ D_k &= \rho\sqrt{k^3}/l_{IDDES} \end{aligned} \tag{13}$$

For the turbulent specific dissipation rate (ω), the production (P_ω), dissipation (D_ω) and cross-diffusion term (CD_ω) are written as:

$$\begin{aligned} P_\omega &= \frac{\rho\gamma}{\mu_t}\tilde{P}_k Re \\ D_\omega &= \beta\rho\omega^2 \\ CD_\omega &= 2\left(1-F_1\right)\frac{\rho\sigma_{\omega 2}}{\omega}\frac{\partial k}{\partial x_j}\frac{\partial \omega}{\partial x_j} \end{aligned} \tag{14}$$

The turbulent viscosity (μ_t) is calculated by:

$$\mu_t = \frac{\rho a_1 k}{\max\left(a_1\omega, SF_2\right)}Re\,, \quad S = \sqrt{S_{ij}S_{ij}}\,, \quad S_{ij} = \frac{1}{2}\left(\frac{\partial u_i}{\partial x_j}+\frac{\partial u_j}{\partial x_i}\right) \tag{15}$$

The blending functions F_1 and F_2 are given by:

$$\begin{aligned} F_1 &= \tanh\left(arg_1^4\right) \\ F_2 &= \tanh\left(arg_2^2\right) \\ arg_1 &= \min\left[\max\left(\frac{\sqrt{k}}{\beta^*\omega d}, \frac{500\mu}{\rho d^2\omega}\frac{1}{Re}\right), \frac{4\rho k\sigma_{\omega 2}}{CD_{k\omega}d^2}\right] \\ arg_2 &= \max\left(\frac{2\sqrt{k}}{\beta^*\omega d}, \frac{500\mu}{\rho d^2\omega}\frac{1}{Re}\right) \\ CD_{k\omega} &= \max\left(2\frac{\rho\sigma_{\omega 2}}{\omega}\frac{\partial k}{\partial x_j}\frac{\partial \omega}{\partial x_j}, 1\times 10^{-10}\right) \end{aligned} \tag{16}$$

The SST model coefficients are blended by:

$$\begin{aligned} \sigma_k &= F_1\sigma_{k1} + \left(1-F_1\right)\sigma_{k2}\,, \quad & \sigma_\omega &= F_1\sigma_{\omega 1} + \left(1-F_1\right)\sigma_{\omega 2} \\ \gamma &= F_1\gamma_1 + \left(1-F_1\right)\gamma_2\,, & \beta &= F_1\beta_1 + \left(1-F_1\right)\beta_2 \end{aligned} \tag{17}$$

Closure coefficients:

$$\begin{aligned} &\beta^* = 0.09, \quad \sigma_{k1} = 0.85, \quad \sigma_{k2} = 1.0, \quad \beta_1 = 0.075, \quad \beta_2 = 0.0828 \\ &\sigma_{\omega 1} = 0.5, \quad \sigma_{\omega 2} = 0.856, \quad \gamma_1 = \frac{5}{9}, \quad \gamma_2 = 0.44, \quad a_1 = 0.31 \end{aligned} \tag{18}$$

The IDDES turbulence model length scale (l_{IDDES}) is defined as a function of RANS and LES length scale using the blending function $\tilde{f}_d$. Unlike the SA-IDDES turbulence model, the fundamental empirical constant, C_{DES}, is also blended using the SST blending function F_1. The IDDES length scale is written as:

$$\begin{aligned} l_{IDDES} &= \tilde{f}_d\left(1+f_e\right)l_{RANS} + \left(1-\tilde{f}_d\right)l_{LES} \\ l_{LES} &= C_{DES}\Delta \\ l_{RANS} &= \frac{\sqrt{k}}{\beta^*\omega} \\ C_{DES} &= F_1 C_{DES1} + \left(1-F_1\right)C_{DES2} \end{aligned} \tag{19}$$

The sub-grid length scale (Δ) depends on the nearest wall distance (d) and the maximum edge length of the cell (Δ_{max}). It is given by:

$$\Delta = \min\left(C_w \max\left[d, \Delta_{max}\right], \Delta_{max}\right) \tag{20}$$

The blending function $\tilde{f}_d$ is calculated using the following relations:

$$\begin{aligned}
\tilde{f}_d &= \max\left(\left(1 - f_{dt}\right), f_b\right) \\
f_{dt} &= 1 - \tanh\left[\left(C_{dt1} r_{dt}\right)^{C_{dt2}}\right] \\
r_{dt} &= \frac{\nu_t}{\kappa^2 d^2 \sqrt{0.5\left(S^2 + \Omega^2\right)}} \frac{1}{Re} \\
f_b &= \min\left(2\exp\left(-9\alpha^2\right), 1.0\right) \\
\alpha &= 0.25 - d/\Delta_{max}
\end{aligned} \tag{21}$$

The elevation function f_e is computed as follow:

$$\begin{aligned}
f_e &= f_{e2} \max\left(\left(f_{e1} - 1.0\right), 0.0\right) \\
f_{e1} &= \begin{cases} 2\exp\left(-11.09\alpha^2\right), \alpha \geq 0 \\ 2\exp\left(-9.0\alpha^2\right), \alpha < 0 \end{cases} \\
f_{e2} &= 1 - \max\left(f_t, f_l\right) \\
f_t &= \tanh\left(\left(C_t^2 r_{dt}\right)^3\right) \\
f_l &= \tanh\left(\left(C_l^2 r_{dl}\right)^{10}\right) \\
r_{dl} &= \frac{\nu}{\kappa^2 d^2 \sqrt{0.5\left(S^2 + \Omega^2\right)}} \frac{1}{Re}
\end{aligned} \tag{22}$$

Additional model constants for IDDES:

$$\begin{aligned}
C_w &= 0.15, \quad C_{dt1} = 20, \quad C_{dt2} = 3, \quad \kappa = 0.41 \\
C_t &= 1.87, \quad C_l = 5.0, \quad C_{DES1} = 0.78, \quad C_{DES2} = 0.61
\end{aligned} \tag{23}$$

IV. Implicit Time Accurate Flow Solver

To solve the Navier-Stokes equations along with the turbulence model in a fully coupled manner, their time-dependent form is first control volume integrated and semi-discretized as:

$$\frac{\partial \mathbf{Q}}{\partial t} = -\frac{1}{\Delta V} \oint_S \mathbf{R}_F . \mathrm{d}\mathbf{s} + \mathbf{D} \tag{24}$$

where, $\mathbf{R}_F$ is the net flux vector discretized in the space and $\mathbf{D}$ is the contribution of the source term.

Following Jameson's dual time stepping method [9], a pseudo temporal term $\partial \mathbf{Q}/\partial \tau$ is added to the left-hand side of Eq. (24). The physical temporal term ($\partial \mathbf{Q}/\partial t$) is discretized using the three-point backward differencing scheme at the physical time levels $n+1$, n and $n-1$. The pseudo temporal term is discretized on two pseudo time-steps (i.e. $m+1$ and m) at the same physical time-step $n+1$. The final formulation of this dual time stepping scheme is given by:

$$\left[\left(\frac{1}{\Delta\tau} + \frac{1.5}{\Delta t}\right) I - \left(\frac{\partial \mathbf{RHS}}{\partial \mathbf{Q}}\right)^{n+1,m}\right] \Delta \mathbf{Q}^{n+1,m+1} = \mathbf{RHS}^{n+1,m} - \frac{3\mathbf{Q}^{n+1,m} - 4\mathbf{Q}^n + \mathbf{Q}^{n-1}}{2\Delta t} \tag{25}$$

where,

$$\mathbf{RHS} = -\frac{1}{\Delta V} \oint_S \mathbf{R}_F \mathrm{d}\mathbf{s} + \mathbf{D} \tag{26}$$

In each physical time step, the solution is converged when $\Delta \mathbf{Q}^{n+1,m+1} \rightarrow 0$ and therefore it has no influence on the solution accuracy.

The Roe flux differencing scheme mentioned in refs. [10, 11] is extended for a two-equation turbulence model in a 3D compressible Navier-Stokes solver. In the case of subsonic flat plate and NACA 0012 post-stall flow, the fifth-order WENO scheme for inviscid fluxes and the fourth-order central differencing scheme for viscous fluxes are used. For the wall-mounted hump case, the third-order WENO for inviscid fluxes and the second-order central differencing for viscous terms are used.

V. Boundary Conditions

For the subsonic inlet with specified stagnation variables BC, the stagnation quantities (i.e. Total Pressure and Total Temperature) are specified along with two flow angles. A velocity component is extracted from the inner domain to calculate the other velocity components, density and total internal energy at the boundary.

For the subsonic inlet with velocity specified BC, velocity components along with the density are specified at the boundary whereas the static pressure is extrapolated from the inner domain to calculate the total internal energy at the boundary.

For SST based models, a turbulence quantity is defined either in terms of the turbulence intensity (I) and the turbulence viscosity ratio (μ_t/μ) or in terms of a multiple of small free-stream values. The normalized form of these quantities is written as:

$$\begin{aligned} \text{Option-1: } k_\infty &= \frac{3}{2}\left(U_\infty I\right)^2 & \text{Option-2:} \quad k_\infty &= 9\times10^{-9}c_\infty^2 \\ \omega_\infty &= \frac{\rho_\infty}{\beta^*}\frac{k_\infty}{\mu_\infty}\left(\frac{\mu_t}{\mu}\right)_\infty^{-1} Re & \omega_\infty &= 1\times10^{-6}\frac{c_\infty^2\rho_\infty}{\mu_\infty}Re \end{aligned} \tag{27}$$

where, c_∞ is the free-stream speed of sound. The conservative form of BC for a turbulence quantity can be obtained by multiplying it with the density at the corresponding phantom cell. With SST based models, the contribution of turbulence kinetic energy is added to the total energy.

For the subsonic outlet BC, the static pressure (p) is specified whereas the four primitive variables and turbulence quantities are extrapolated from the inner domain.

At the wall, no-slip adiabatic wall boundary condition is specified. For this non-reflective BC, the negative of first interior cell velocity is defined at the ghost cell. This leads to the zero velocity at the wall. For inviscid fluxes, the contravariant velocity on the boundary is set to zero. For SST based models, a turbulence quantity is specified at the phantom cell considering $y^+ < 1$ for the first cell grid spacing near the wall. The normalized turbulence quantity on 1st cell near wall is given as:

$$\begin{aligned} k_{ghost} &= -k_1 \\ \omega_{ghost} &= -\omega_1 + 2\frac{60\mu}{\rho_1\beta_1 d^2}\frac{1}{Re} \end{aligned} \tag{28}$$

VI. Results

A. Subsonic Flat Plate

The standard zero pressure gradient subsonic flat plate case is simulated first to validate the implementation of SST-IDDES model. This case is also used to study the grid refinement effect on the velocity distribution in the boundary layer and the MSD problem. The overall dimension of geometry on a 2D plane is shown in Fig. 1. In the span-wise direction, the length of 0.01 is used. For a numerical simulation with SST based models, Reynolds number (Re_L) of 1.615×10^7 based on the flat plate length and Mach number (M_∞) of 0.6 are used.

The ambiguous grid used to investigate the MSD problem is shown in Fig. 2. The mesh is refined systematically in the stream-wise direction to purposefully create the wall parallel cell length much smaller than the boundary layer thickness. Near the inlet, $\Delta_x = 1.5\delta_L$ grid spacing is used. With the systematic grid refinement, the wall parallel spacing near the outlet is $\Delta_x = 0.026\delta_L$. In the span-wise direction, $\Delta_z = 0.1\delta_L$ is used. The grid spacing normal to the wall ensures y^+ of 0.5.

The boundary condition at the inlet, outlet, top and bottom face is shown in Fig. 1. On two side faces, the zero-gradient boundary condition is specified. Turbulence quantities are defined based on Option-2. The steady-state simulation is performed with a pseudo time step based on the CFL number of 5.

The predicted profile of stream-wise velocity, turbulent viscosity and turbulent shear stress with SST based models is extracted at the outlet boundary. The predicted dimensionless velocity with SST based models is plotted as a function of wall units on a logarithmic axis and compared against the law of wall, Fig. 3(a). The predicted profile with both models agrees well with the law of wall and the SST-IDDES model does not exhibit the MSD problem. The predicted velocity profile between the SST based models exhibits a minor difference in the far-field. The distribution of nondimensional turbulent shear stress and turbulent viscosity in the boundary layer is shown in Fig. 3(b). The predicted dimensionless

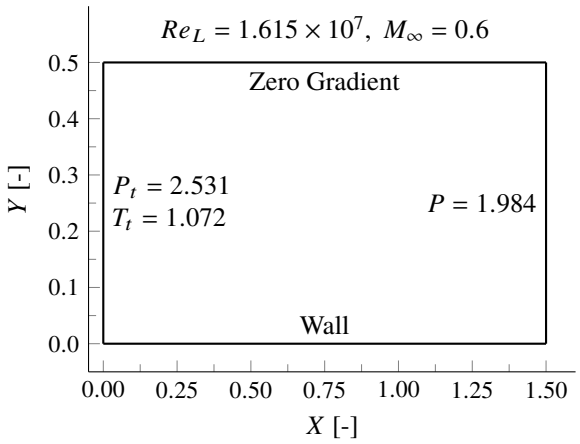

Fig. 1 Geometry and Boundary conditions

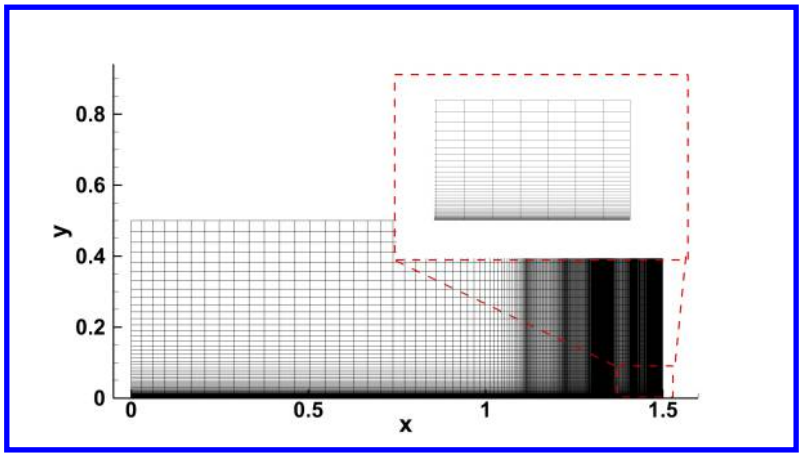

Fig. 2 Mesh overview

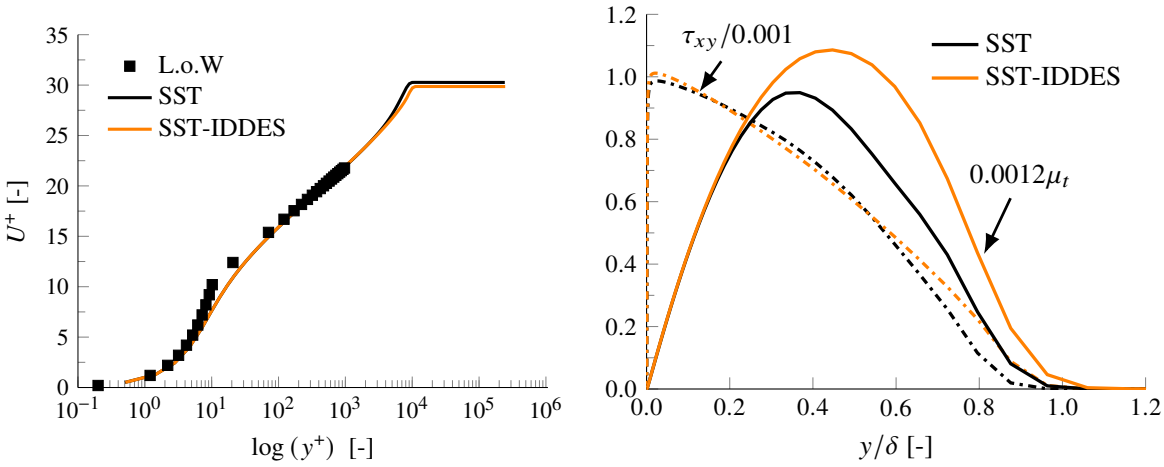

(a) Law of wall **(b) Turbulent shear stress and viscosity distribution**

Fig. 3 Distributions in flat plate boundary layer

eddy viscosity with the SST-IDDES model matches well with the SST model in the inner and a part of the outer boundary layer region. In the remaining outer boundary layer, the SST-IDDES model over-predicts the turbulent viscosity and follows a trend similar to the SST model. However, the predicted Reynolds shear stress of both models agree very well.

B. 2D NASA Wall-Mounted Hump

In 2004, the 2D wall-mounted hump, shown in Fig. 4, was chosen in the NASA CFDVAL2004 workshop to evaluate the capabilities of existing RANS turbulence models in reproducing the flow physics involving separation. The geometry includes the wall-mounted Glauert-Goldschmied body. A summary of the different RANS turbulence models' results with experimental measurement can be found in reference [12]. Most of the RANS turbulence models' results with the steady-state or the unsteady simulation have consistently over-predicted the reattachment point for the baseline case with no flow control. This hump case is selected in the present study as a validation of the SST-IDDES model.

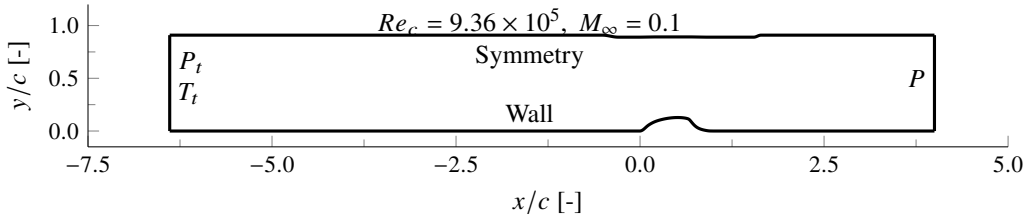

Fig. 4 Geometry and Boundary conditions

Table 1 Computational grids for the NASA Wall-Mounted Hump case

Grid	Size	Δx_{min}	Δy_{min}	Δz_{min}	Δx^+_{min}	Δy^+_{min}	Δz^+_{min}
Mesh-A	205 x 55 x 1	0.0045	2.74×10^{-5}		500	3	
Mesh-B	409 x 109 x 1	0.0023	1.36×10^{-5}		250	1.5	
Mesh-C	817 x 217 x 1	0.0011	6.81×10^{-6}		125	0.76	
Mesh-D	205 x 55 x 25	0.0045	2.74×10^{-5}	0.0083	500	3	930

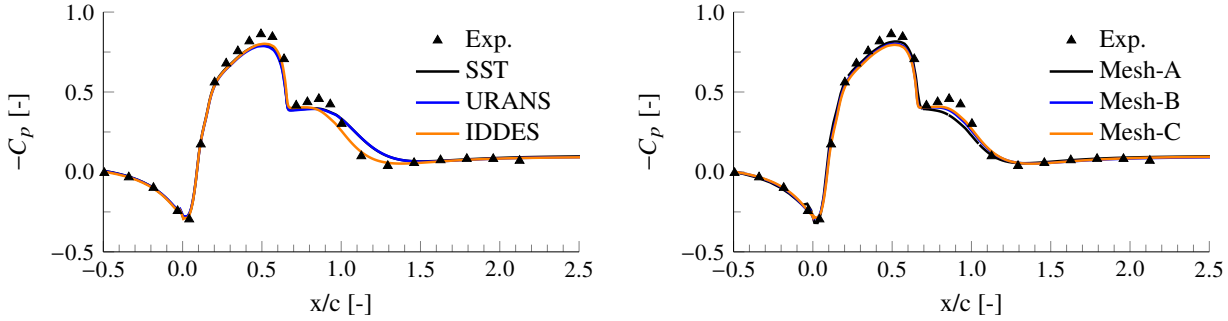

(a) $-C_p$ comparison for Mesh-B **(b) Mesh-independence study with 2-D case**

Fig. 5 $-C_p$ comparison

Fig. 4 shows the 2-D computational domain along with the boundary conditions. Details of various computational grid are given in Table 1. The steady-state and unsteady simulations are carried out mostly on the 2-D computational domain. For the 3-D computation, Mesh-A computational domain is extended by $0.2c$ in the spanwise direction (i.e., Mesh-D) similar to the reference [7]. With the hybrid turbulence model, the inlet boundary condition is still located at $-6.4c$.

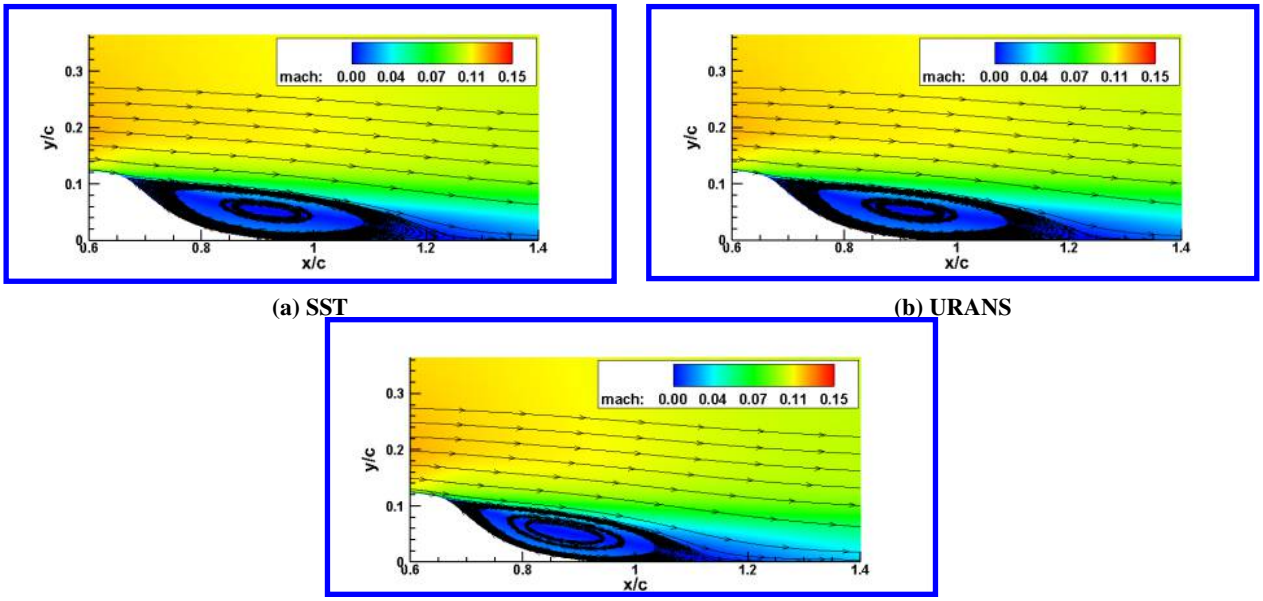

(a) SST (b) URANS

(c) IDDES

Fig. 6 Mach number contours

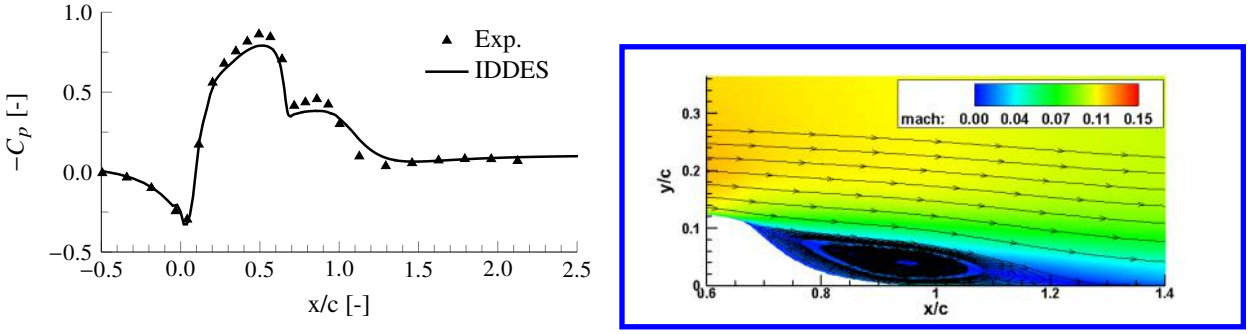

(a) $-C_p$ comparison (b) Spanwise averaged Mach number contour

Fig. 7 Coefficient of pressure and Mach number contour with Mesh-D

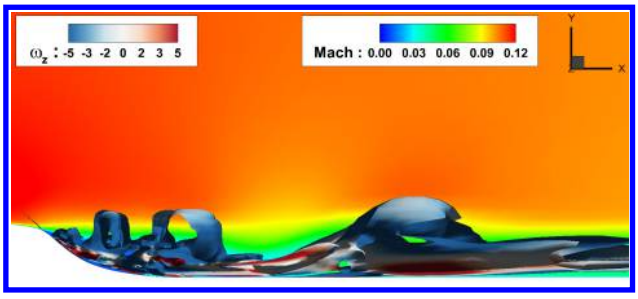

Fig. 8 Instantaneous iso-surfaces of Q-criterion=2 and Mach number contour at $z/c = 0$ with Mesh-D

The stagnation quantities and flow angles are defined at the inlet with 0.077 % freestream turbulence intensity and 0.009 freestream turbulence viscosity ratio. At the outlet, the static pressure is specified. The no-slip wall boundary condition is used at the wall and the symmetry at the top. For the 3-D computation, the periodic boundary condition is employed in the spanwise direction. The simulation is conducted at Reynolds number of 9.36×10^5 based on the hump chord and the freestream Mach number is 0.1. The simulation is started from the uniform flow field. The pseudo time-step

for the steady and unsteady analysis is based on the CFL number of 2, whereas the nondimensional characteristic time-step of 0.0025 is used for the unsteady analysis. The unsteady simulation is carried for 200 nondimensional characteristic time. For the statistical time-averaging with unsteady simulations, initial 125 characteristic time results are discarded to avoid initial flow transition effects.

In Fig. 5, the predicted coefficient of pressure (C_p) is compared with the experimental measurement [13]. For the 2-D simulation with the Mesh-B, the steady-state and URANS results are effectively the same and both over-predict the separation size. The predicted C_p with the IDDES agrees well with the experiment, even in the 2-D simulation. For the mesh-independence study, various 2-D cases are simulated with the IDDES and results are compared against the experiment in Fig. 5(b). With the mesh refinement, a minor difference in C_p is observed between $0.6c$ and $1.1c$.

The 2-D simulation Mach number contours with the Mesh-B using different turbulence models are compared in Fig. 6. The steady and unsteady simulation with the SST model exhibit delayed reattachment of the flow. With these models, the turbulent shear stress is under-predicted which leads to the reduced turbulent mixing and larger flow separation. In the case of IDDES, the prediction of Reynolds shear stress is improved due to the eddy resolution in LES mode and therefore early flow reattachment. The IDDES model predicts the reattachment point at $x/c \approx 1.16$ in contrast to $x/c \approx 1.27$ with the SST turbulence model.

The predicted pressure coefficient with the 3-D simulation using the IDDES is compared with the experimental measurement in Fig. 7(a). The flow separation region does not agree as well as the 2-D simulation results and shows a 3-D vortical flow instability. The 3-D vortical flow structures are shown in Fig. 8 with the instantaneous iso-surfaces of Q-criterion colored by the vorticity about z direction. It is observed by many researchers [7, 14, 15] that the LES mode transition is delayed in this particular case with the present LES length scale definition. To overcome this grey area mitigation problem, researchers have devised techniques like using a modified length scale (like shear layer adaptive, vorticity based, etc.), synthetic turbulence generator, zonal hybrid RANS/LES model, etc. In the present study, the authors use the standard LES length scale based on Δ_{max} and therefore the reattachment point is delayed.

C. NACA 0012 Airfoil Stalled flow

The massive flow separation of NACA 0012 stalled flow contains large eddies of the size comparable to the geometry scale. The accurate prediction of such flow-field necessitates resolving large-energy containing eddies instead of modeling. Therefore, this case is used by many researchers to evaluate the effectiveness of a hybrid model over a URANS. Shur et al. investigated this case with the SA-DES turbulence model and the experimental results can be found in the ref. [16]. This case is selected to be simulated using the SST-IDDES model.

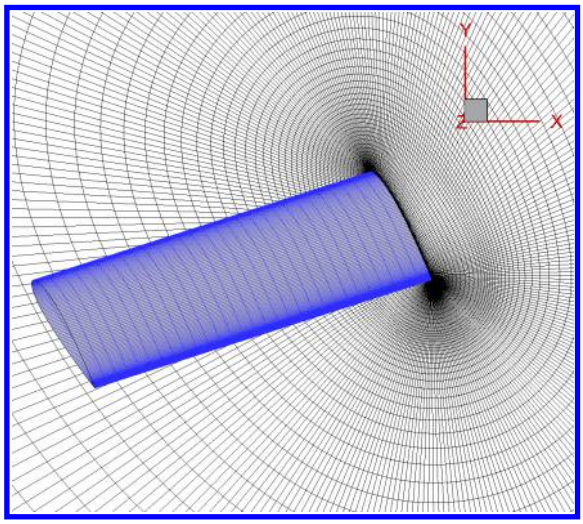

Fig. 9 Computational Grid for NACA 0012 airfoil

The computational grid contains about 0.84 millions of hexahedron cells with 289 nodes around the airfoil, 101 nodes normal to the wall and 30 nodes in the spanwise direction. In wall units, the grid parameters are $(\Delta x^+,\ \Delta y^+,\ \Delta z^+)$ = (6.6–894, 1, 1720). The O topology mesh is used around the airfoil as it ensures a highly orthogonal grid near the wall. The computational domain is extended to 80 times the airfoil chord length away from the

wall and its size in the spanwise direction is one chord length. Fig. 9 shows the computational grid used in the present study.

The subsonic inlet with the velocity specified BC is used at the inlet with turbulence quantities as a multiple of small freestream values (i.e., Option-2). The static pressure is defined at the outlet. At the wall, the no-slip wall boundary condition is used. In the spanwise direction, the periodic boundary condition is specified. The present simulation is conducted at the Reynolds number of 1.3×10^6 based on one airfoil chord length and the freestream Mach number is 0.5. For the unsteady calculation, the simulation is started from the uniform flow field with the nondimensional characteristic time-step of 0.02 and the pseudo time-step based on the CFL number of 2.5. The simulation is carried out for 480 nondimensional characteristic time.

With the aforementioned numerical set-up, the case is simulated at two different angles of attacks using the SST and SST-IDDES models. Fig. 10 shows the predicted lift- and drag-coefficient signal with both models. The SST URANS model significantly over-predicts both the lift and drag coefficient. For the statistical time-averaging, initial 200 dimensionless time results are discarded to avoid initial flow transition effects. The change in statistical time-averaged quantities over the last 280 nondimensional time is also shown in Fig. 10. These time-averaged quantities are compared with the experimental measurement in Table 2. The SST-IDDES results agree well with the experiment, significantly more accurate than the SST URANS model. The slight over-prediction of lift coefficient at 45° for IDDES is similar to the one observed by Patel et al. [17] using the SA based hybrid models.

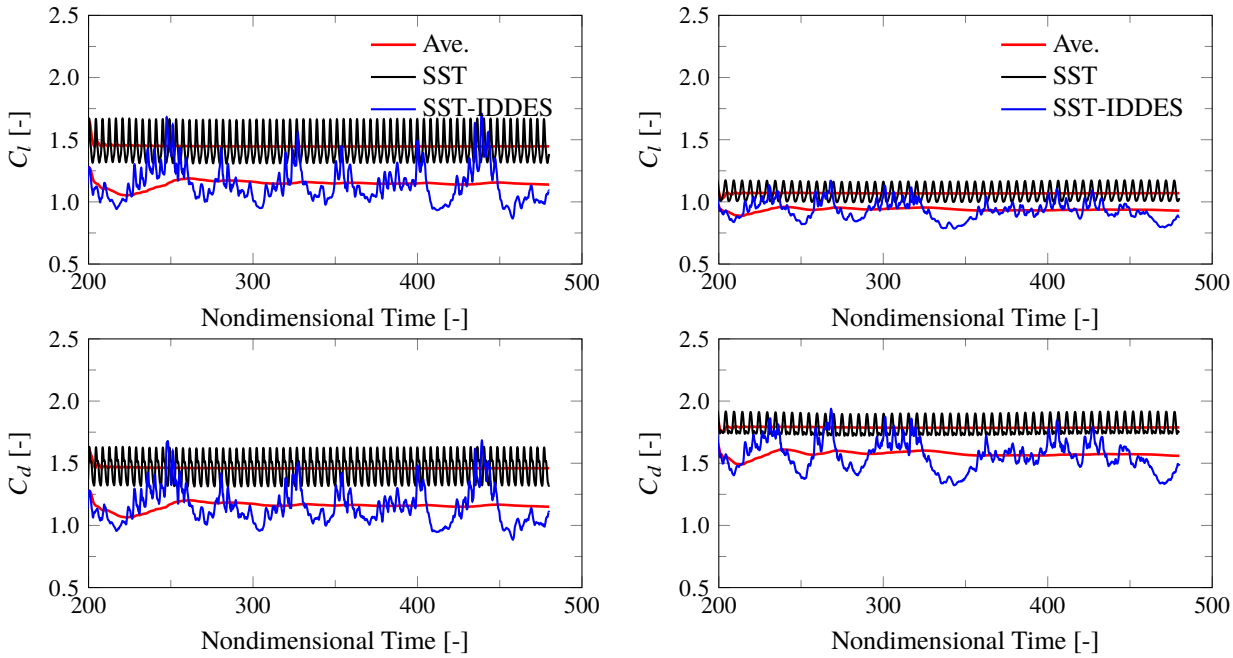

(a) AoA = 45° **(b) AoA = 60°**

Fig. 10 Lift and Drag coefficient vs Time for NACA 0012 airfoil

The spectral content based on the lift coefficient at different angles of attacks is shown in Fig. 11. The abscissa represents the Strouhal number (St) and the ordinate represents the power content. The peak in power content with the SST is distinct and shows multiple frequencies beating phenomenon. This also represents the organized vortex-shedding from the airfoil surface. However, the SST-IDDES model shows the broadband frequency with the first dominant peak close to the SST model. The higher energy spectra with the SST-IDDES model suggests the resolution of eddies.

The effect of different spanwise extent is investigated using the SST-IDDES model at 60° angle of attack. For this study, three different spanwise extents are considered with the same grid parameters to avoid the influence of different Δz^+ in the spanwise direction. The predicted statistical time-averaged lift and drag coefficients vary less than 3 % from $1c$ to $3c$ spanwise extent, as shown in Fig. 12(a). The spectral content based on the lift coefficient is compared in Fig. 12(b). The higher lift coefficient prediction with $1c$ extent is evident from the higher spectral content. With the larger spanwise extent, the peak in spectral content near St of 0.2 is more prominent.

Table 2 C_l and C_d comparison for NACA 0012

AoA	Turbulence Model	C_l	C_d
45°	Experimental [16]	1.097	1.180
	URANS	1.446	1.460
	IDDES	1.139	1.150
60°	Experimental [16]	0.930	1.640
	URANS	1.070	1.788
	IDDES	0.952	1.610

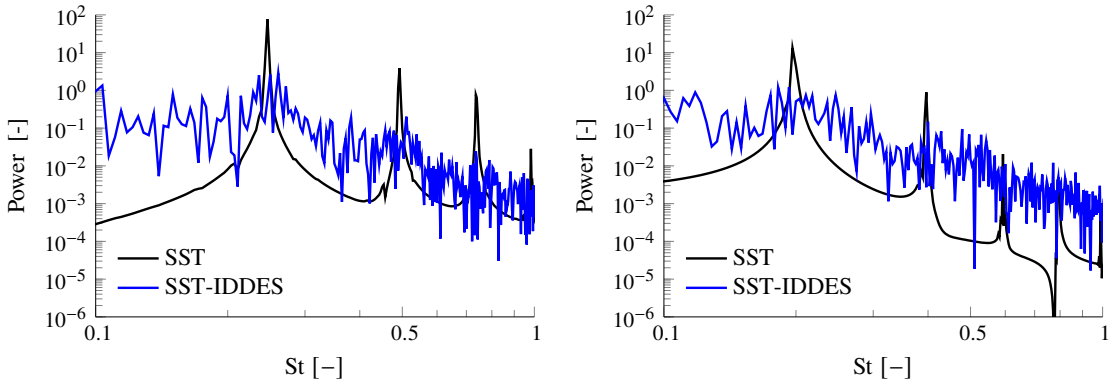

(a) AoA = 45° **(b) AoA =** 60°

Fig. 11 Spectral content based on C_l with Span = $1c$

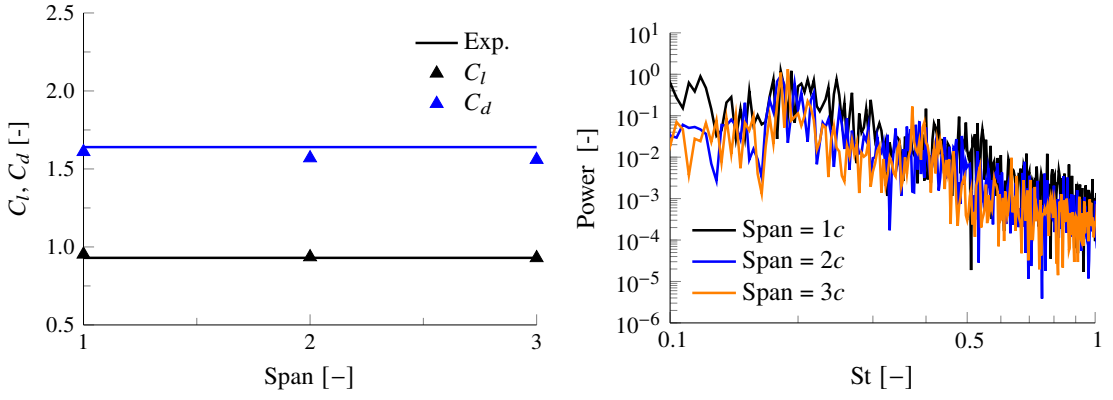

(a) Aerodynamic performance **(b) Spectral content based on C_l**

Fig. 12 Effect of spanwise domain extent on IDDES results at AoA = 60°

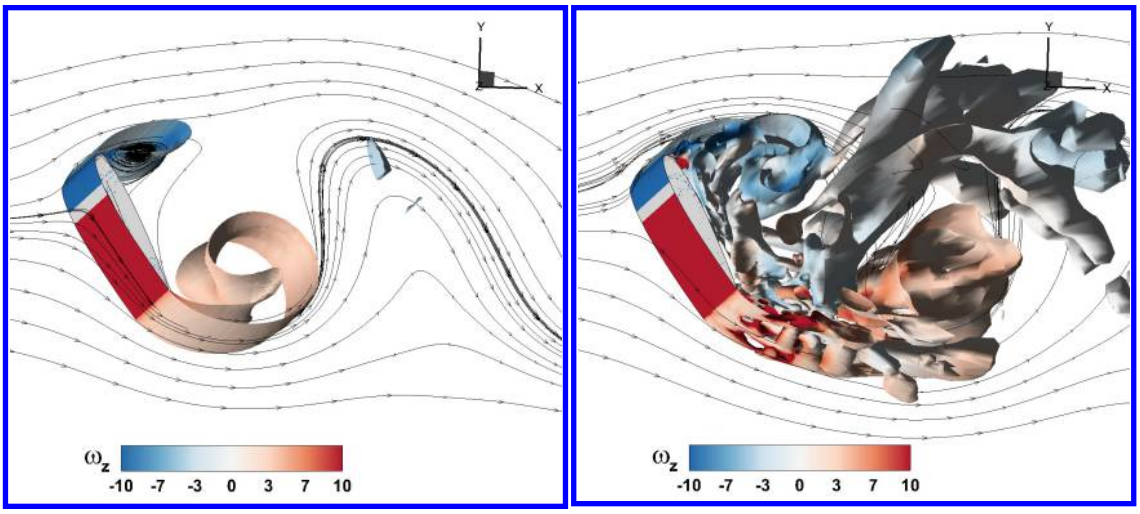

(a) URANS **(b) IDDES**

Fig. 13 Instantaneous iso-surfaces of Q-criterion=5 and streamlines

Fig. 13 depicts the iso-surfaces of Q-criterion colored by the vorticity about z direction and streamlines with $1c$ spanwise extent for both models. The vortex structure with the URANS is dominantly 2-D and organized as compared to the 3-D, more small structures resolved by the IDDES, representing the LES like flow structures.

VII. Conclusions

The fully coupled SST-IDDES turbulence model is implemented in a 3D compressible Navier-Stokes solver and validated with different cases to study its efficacy in resolving flow separation. For the standard zero pressure gradient subsonic flat plate case, the distribution of flow properties in the boundary layer matches well with its base model and does not exhibit the mean stress depletion problem with the ambiguous grid.

In the case of NASA wall-mounted hump, the hybrid turbulence model results agree well with experiment as compared to the SST RANS model. The flow separation size prediction improves with the IDDES due to eddy resolution in the LES mode. The steady-state and URANS simulation with the SST over-predicts the separation size due to the under-prediction of turbulent shear stresses.

For the massive flow separation case with NACA 0012 airfoil post-stall flow, the predicted aerodynamic performance is in close agreement with the experiment as compared with the URANS. The effect of the spanwise extent on the IDDES results is in the range of engineering tolerance. The IDDES model obtains much more accurate quantitative results and captures a more realistic 3-D, small scale turbulent flow structure.

Acknowledgments

We would like to thank the Center for Computational Science at University of Miami, Coral Gables for providing computational resources.

References

[1] Spalart, P. R., Jou, W.-H., Strelets, M., and Allmaras, S., "Comments on the Feasibility of LES for Wings, and on a Hybrid RANS/LES Approach," 1997.

[2] Strelets, M., *Detached eddy simulation of massively separated flows*, 2001. doi:10.2514/6.2001-879, URL `https://arc.aiaa.org/doi/abs/10.2514/6.2001-879`.

[3] Menter, F., and Kuntz, M., *Adaptation of Eddy-Viscosity Turbulence Models to Unsteady Separated Flow Behind Vehicles*, 2004, Vol. 19, pp. 339–352. doi:10.1007/978-3-540-44419-0_30.

[4] Spalart, P. R., Deck, S., Shur, M. L., Squires, K. D., Strelets, M. K., and Travin, A. K., "A New Version of Detached-eddy

Simulation, Resistant to Ambiguous Grid Densities," *Theoretical and Computational Fluid Dynamics*, Vol. 20, No. 3, 2006, p. 181. doi:10.1007/s00162-006-0015-0, URL https://doi.org/10.1007/s00162-006-0015-0.

[5] Menter, F. R., Kuntz, M., and Langtry, R., "Ten Years of Industrial Experience with the SST Turbulence Model," *Turbulence Heat and Mass Transfer*, Vol. 4, 2003, pp. 625–632.

[6] Shur, M. L., Spalart, P. R., Strelets, M. K., and Travin, A. K., "A hybrid RANS-LES approach with delayed-DES and wall-modelled LES capabilities," *International Journal of Heat and Fluid Flow*, Vol. 29, No. 6, 2008, pp. 1638 – 1649. URL http://www.sciencedirect.com/science/article/pii/S0142727X08001203.

[7] Gritskevich, M., Garbaruk, A., Schütze, J., and Menter, F., "Development of DDES and IDDES Formulations for the $k-\omega$ Shear Stress Transport Model," *Flow, Turbulence and Combustion*, Vol. 88, 2012. doi:10.1007/s10494-011-9378-4.

[8] Zha, G.-C., and Bilgen, E., "Numerical Study of Three-Dimensional Flows Using Unfactored Upwind-Relaxation Sweeping Algorithm," *J. Comput. Phys.*, Vol. 125, No. 2, 1996, pp. 425–433. doi:10.1006/jcph.1996.0104, URL http://dx.doi.org/10.1006/jcph.1996.0104.

[9] Jameson, A., "Time dependent calculations using multigrid, with applications to unsteady flows past airfoils and wings," Fluid Dynamics and Co-located Conferences, American Institute of Aeronautics and Astronautics, 1991. doi:10.2514/6.1991-1596, URL https://doi.org/10.2514/6.1991-1596.

[10] Zha, G., "Comparative study of upwind scheme performance for entropy condition and discontinuities," 14th Computational Fluid Dynamics Conference, American Institute of Aeronautics and Astronautics, 1999. doi:10.2514/6.1999-3348, URL https://doi.org/10.2514/6.1999-3348.

[11] Wang, B., and Zha, G., "Comparison of a Low Diffusion E-CUSP and the Roe Scheme for RANS Calculation," 46th AIAA Aerospace Sciences Meeting and Exhibit, American Institute of Aeronautics and Astronautics, 2008. doi:10.2514/6.2008-569, URL https://doi.org/10.2514/6.2008-569.

[12] Rumsey, C., Gatski, T., Sellers, W., Vatsa, V., and Viken, S., *Summary of the 2004 CFD Validation Workshop on Synthetic Jets and Turbulent Separation Control*, 2004. doi:10.2514/6.2004-2217, URL https://arc.aiaa.org/doi/abs/10.2514/6.2004-2217.

[13] "2D NASA Wall-Mounted Hump Separated Flow Validation Case," , 2004. URL https://turbmodels.larc.nasa.gov/nasahump_val.html.

[14] Guseva, E. K., Garbaruk, A. V., and Strelets, M. K., "Application of DDES and IDDES with shear layer adapted subgrid length-scale to separated flows," *Journal of Physics: Conference Series*, Vol. 769, 2016, p. 012081. doi:10.1088/1742-6596/769/1/012081.

[15] Kiris, C. C., Stich, D., Housman, J. A., Kocheemoolayil, J. G., Barad, M. F., and Cadieux, F., *Application of Lattice Boltzmann and Navier-Stokes Methods to NASA Wall Mounted Hump*, 2018. doi:10.2514/6.2018-3855, AIAA 2018-3855.

[16] Shur, M. L., Spalart, P. R., Strelets, M. K., and Travin, A. K., "Detached-eddy simulation of an airfoil at high angle of attack," *Engineering Turbulence Modelling and Experiments 4*, edited by W. Rodi and D. Laurence, Elsevier Science Ltd, Oxford, 1999, pp. 669 – 678. doi:https://doi.org/10.1016/B978-008043328-8/50064-3, URL http://www.sciencedirect.com/science/article/pii/B9780080433288500643.

[17] Patel, P., Yang, Y., and Zha, G., "Scale Adaptive Simulation of stalled NACA 0012 airfoil using high order schemes," *AIAA Aviation 2019 Forum*, 2019. doi:10.2514/6.2019-3527, URL https://arc.aiaa.org/doi/abs/10.2514/6.2019-3527.